



Article

Synthesis and Properties of Electrodeposited Ni–Co/WS₂ Nanocomposite Coatings

Yang He ^{1,*}, Shuncai Wang ², Wanting Sun ³, Philippa A.S. Reed ⁴  and Frank C. Walsh ² 

¹ Centre for Composite Materials and Structures, Harbin Institute of Technology, Harbin 150080, China

² National Centre for Advanced Tribology at Southampton (nCATS), University of Southampton, Southampton SO17 1BJ, UK; wangs@soton.ac.uk (S.W.); F.C.Walsh@soton.ac.uk (F.C.W.)

³ School of Materials Science and Engineering, Harbin Institute of Technology, Harbin 150001, China; sunwt_hit@126.com

⁴ Engineering Materials and Surface Engineering, University of Southampton, Southampton SO17 1BJ, UK; P.A.Reed@soton.ac.uk

* Correspondence: yang.he@hit.edu.cn

Received: 17 January 2019; Accepted: 13 February 2019; Published: 25 February 2019



Abstract: Ni–Co coatings have gained widespread attention due to their potential in replacing hard chromium deposits (which have traditionally utilized toxic and corrosive chromic acid baths). A major challenge is to lower the high coefficient of friction of coated surfaces against steel, under dry sliding conditions. In this research, low friction Ni–Co/WS₂ nanocomposite coatings have been prepared by a convenient, one-pot electrodeposition from aqueous Ni–Co plating baths containing WS₂ particles. The embedment of the WS₂ lubricants is found to reduce the friction coefficient of coating significantly, and an ultra-low friction coefficient of 0.16 is obtained for the coating having a WS₂ content of 7.1 wt.%. Morphology and composition characterization of wear tracks reveal that the formation of a WS₂-rich lubricating tribofilm on the contact surfaces is beneficial to a low friction coefficient and good oxidation resistance. The wettability of electrodeposited coatings was also investigated. Compared to pure Ni–Co coating, the Ni–Co/7.1 wt.% WS₂ coating has an excellent hydrophobicity with a high water contact angle (WCA) of 157°, due to a rough surface with dual scale protrusions and the low surface energy of WS₂.

Keywords: Ni–Co; WS₂; hydrophobicity; low friction; nanocomposite

1. Introduction

As one of the most promising alternatives for replacement of hard-chromium coatings, Ni–Co coatings have numerous advantages, including high hardness, good adhesion, superior wear and corrosion resistance. These deposits have been widely used in tribological applications [1–3]. A favored method for the preparation of Ni–Co alloy/composite coatings is electrodeposition, which is facile, reproducible, readily controlled and suitable for industrial scale-up [4]. Over the last three decades, considerable research studies have focused on tailoring the microstructure and tribological properties of Ni–Co coating via control of the electrolyte composition, electrodeposition conditions and heat treatment temperature [5–8].

A coating offering low friction against a steel counterpart can reduce the emission of long-lived greenhouse gases, including carbon dioxide (CO₂), nitrogen oxides (N₂O and NO₂) and methane (CH₄). The attempt to produce such a coating has attracted increasing attention in both fundamental research and industrial practice. Ni based metallic coatings, however, possess a range of high friction coefficients (in the range of 0.4 to 0.7) against steel under dry friction conditions, which cannot fulfil economic expectations and meet the rising demands for environmental protection. Composite coatings

of solid lubricants in a metallic matrix, for example, CNTs [9,10], graphite [11,12], MoS₂ [13], WS₂ [14] and reduced graphene oxide [15], have been widely developed to provide enhanced tribological properties (i.e., low friction, chemical inertness, good wear and corrosion resistance).

As a distinct solid lubricant, WS₂ has a very low coefficient of friction (approx. 0.01) owing to the facile shear of weak interlayer bonds (bound by van der Waal's forces) between layers. Furthermore, it has a good thermal stability up to 594 °C. These characteristics make WS₂ very suitable as a friction modifier in metallic coatings. Metal-WS₂ composite coatings with low friction coefficient and/or good wear resistance have been intensively prepared via electrodeposition over recent years. Tenne et al. [14] electrodeposited WS₂ particle impregnated Ni films on archwires, which showed a reduction in frictional force up to 60% in comparison to uncoated archwires. García-Lecina et al. [16] reported an electrodeposited Ni-WS₂ coating with a stable friction coefficient of 0.4 against steel. Tudela et al. [17] further improved the mechanical strength of the electrodeposited Ni-WS₂ coating to enhance bath agitation. Das et al. [18] demonstrated that pulse current electrodeposited Ni-WS₂ coating showed a very low friction coefficient of 0.12. In a previous study, we investigated the self-lubricating properties of an electrodeposited Ni-P/WS₂ composite coating [19]. Research on the promising combination of ceramic WS₂ lubricants and Ni-Co coatings is very limited.

Superhydrophobic coatings have wide potential applications in, e.g., self-cleaning, anti-icing, oil/water separation, anti-corrosion, anti-fouling, energy saving, and medical implants. Recently, superhydrophobic WS₂ composite surfaces including Ni/WS₂ [20] and Ni-P/WS₂ [19] have been readily obtained by electrodeposition without the need for expensive equipment or a specialized reaction environment.

In this study, we present work on the fabrication of low friction Ni-Co/WS₂ composite coatings via facile, one-pot electrodeposition in a modified Watts Nickel bath. The variations of microstructure, tribological and hydrophobic properties, which are dependent on the WS₂ content of the coating, are systematically investigated. In sliding friction studies, the wear tracks are thoroughly characterized and the self-lubricating mechanism is discussed in detail.

2. Experimental Details

2.1. Sample Preparation

Analytical reagents and distilled water were used to prepare the plating solution. The Ni-Co/WS₂ composite coating was deposited from an electrolyte bath consisting of NiSO₄·6H₂O (200 g L⁻¹), NiCl₂·6H₂O (40 g L⁻¹), CoSO₄·7H₂O (40 g L⁻¹), boric acid (30 g L⁻¹), saccharin (2 g L⁻¹), cetyltrimethylammonium bromide (CTAB) (0.1 g L⁻¹) and WS₂ particles (1, 5, 10, 15, 25 g L⁻¹). The pH value of the solution was maintained at 4. To improve the dispersion, the solution was placed in an ultrasonic water bath for 15 min before electrodeposition.

A Tti QL355T power station (Cambridge, UK) was chosen as the power source. The coatings were deposited at 3 A dm⁻² for 45 min. The bath temperature was maintained at 45 °C by a Grant LTD6G water bath (Cambridge, UK). The electrolyte was continuously stirred by a PTFE-coated magnetic stirrer bar (6 mm diameter × 30 mm length) at 1.67 s⁻¹. The anode was a Ni sheet (purity 99.5%) with a thickness of 1 mm, supplied by Goodman Alloys Ltd. (Yorkshire, England). The cathode substrate was 3 mm thick AISI 1020 mild steel supplied by Goodman Alloys Ltd. (Yorkshire, UK) with a hardness of 150 HV. Both the anode and cathode were cut to a size of 80 mm × 10 mm. Before electrodeposition, the surfaces were mechanically polished with 400, 800, and 1200 grade waterproof abrasive paper sequentially and then ultrasonically cleaned with acetone to remove contamination. During deposition, the cathode was held vertical and parallel to the anode with an interelectrode gap of 25 mm.

2.2. Characterization

Linear sweep voltammetry (LSV) measurements were performed with an Autolab PGSTA30 system in conjunction with a conventional, three-electrode glass cell. The working electrode was a

rectangular mild steel plate of dimensions 10 and 40 mm, and the counter electrode was a platinum mesh electrode of similar dimensions. All LSV scans were recorded at a scan rate of 10 mV s^{-1} over the potential range of -0.5 V to -1.2 V vs. saturated calomel electrode (SCE).

The surface morphologies of as-deposited coatings and wear tracks were imaged using a JEOL JSM 6500 SEM (Tokyo, Japan), using an applied voltage of 15 kV and a working distance of 10 mm. Using integrated energy dispersive X-ray spectroscopy (Oxford Instruments, Oxford, UK), EDS, quantitative elemental information on samples was examined by the characteristic X-ray emission. The phase structures of the composite coatings were analyzed using a Bruker GADDS diffractometer with $\text{Cu K}\alpha$ radiation, scanned at 0.02 deg s^{-1} over the 2θ range from 10° to 90° .

The friction and wear characteristics of the as obtained coatings were assessed using a reciprocating tribometer (Plint and Parners, Ltd., Wokingham, UK, model TE-77). The experiments were conducted at a constant temperature of 25°C , in the dry sliding condition and at 40% relative humidity. AISI-52100 steel balls (diameter: 6 mm, hardness: 700 HV, R_a : $0.12 \mu\text{m}$) were used as the sliding counter faces. The tests were carried out under a sliding frequency of 1 Hz and a sliding stroke of 2.69 mm for 1000 s. The normal contact load is 5 N and the frictional force is recorded automatically by a piezoelectric transducer. Friction tests on samples were repeated twice to ensure reliability.

Water contact angles (WCA) were determined using a commercial instrument Drop Shape Analysis system (KRÜSS, Hamburg, Germany, model DSA100) with a computer-controlled liquid dispensing system. The values of WCA are taken as an average of five measurements made with $6 \mu\text{L}$ distilled water droplets.

3. Results and Discussions

3.1. Linear Sweep Voltammetric (LSV) Analysis

The LSV method was utilized to analyze the mechanism of the coating formation on substrate. Negative direction, cathodic sweep was performed in the range from 500 to -1300 mV which was selected on the basis of the onset of alloy deposition. The cathodic LSV curve in Figure 1 shows that the reduction current density rises quickly as the potential decreases below -0.93 V , which corresponds to rapid simultaneous deposition of cobalt and nickel. After addition of WS_2 particles in the electrolyte, the LSV curve shows progressive polarization towards a more negative potential value of -1.01 V although the slope of the curve remains almost unchanged. The delay in electrodeposition is in agreement with results in Ni-Co/C nanotubes reported by Liu et al. [21], and can be attributed to the hindrance effect of WS_2 particles adsorbed on the electrode surface. The Ni-Co/ WS_2 plating system with CTAB addition exhibits polarization towards a more positive potential value. This is due to the adsorption of CTAB cationic surfactant molecules on particles, accelerating the codeposition of WS_2 particles into the Ni-Co matrix.

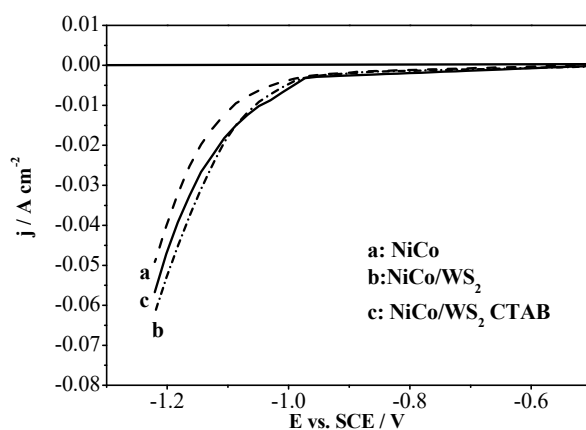


Figure 1. The current density-cathodic potential curves of (state electrode reactions) in Ni-Co and Ni-Co/ WS_2 electrolytes.

3.2. Morphology and Structure

Figure 2 shows the WS₂ platelets with an irregular shape, which have diameters in the range of 80–240 nm. Figure 3 shows the surface morphologies of Ni–Co coating and Ni–Co/WS₂ coatings deposited from baths with different WS₂ concentrations. Compared to the flat morphology of the Ni–Co coating, Ni–Co/WS₂ coatings deposited at a WS₂ concentration of 1 g L^{−1} have a rough surface decorated with nodular protrusions. The density and diameter of the nodular protrusions increased at higher WS₂ concentration in the bath. During electrodeposition, Ni ions are preferably reduced around WS₂ semi conductive particles at the electrode, resulting in a high localized current distribution and the growth of Ni–Co/WS₂ bulges on the deposit surface.

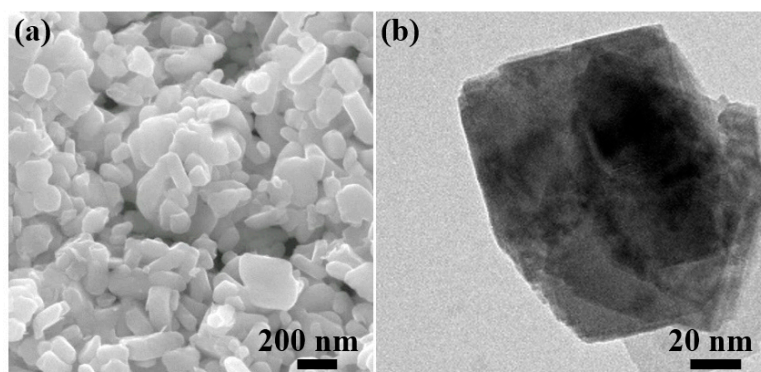


Figure 2. (a) SEM image and (b) TEM image of as-received WS₂ particles.

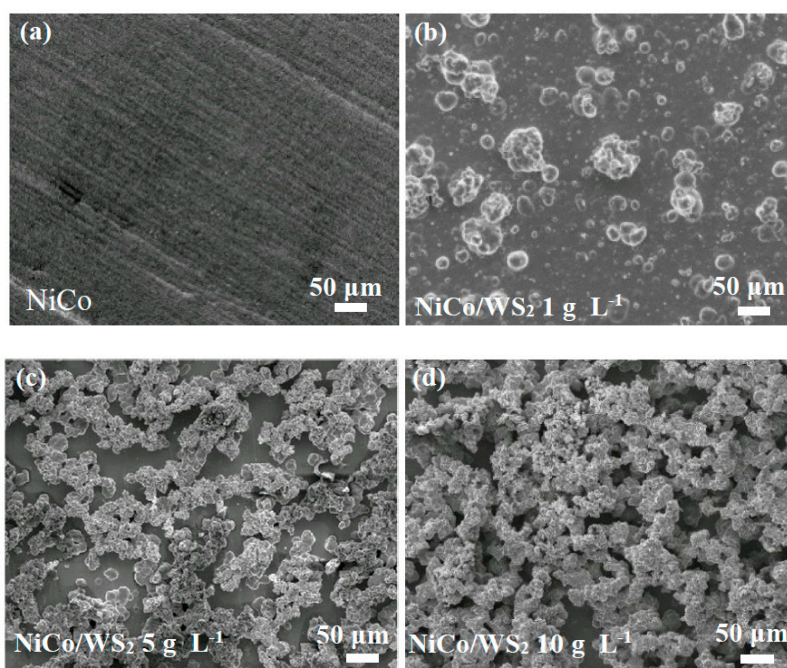


Figure 3. *Cont.*

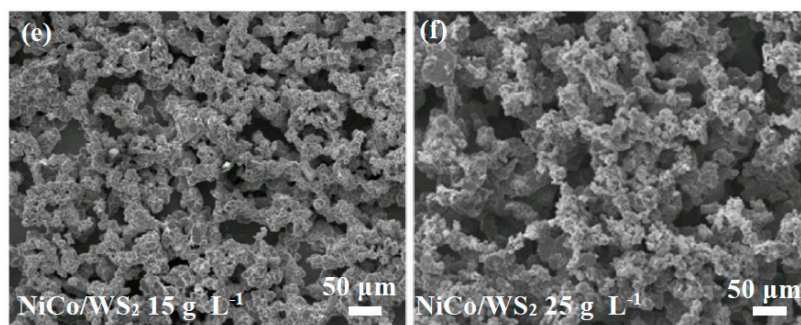


Figure 3. SEM images of the Ni-Co/WS₂ coatings deposited from solutions having controlled WS₂ concentrations: (a) 0 g L^{−1}, (b) 1 g L^{−1}, (c) 5 g L^{−1}, (d) 10 g L^{−1}, (e) 15 g L^{−1} and (f) 25 g L^{−1}.

The XRD patterns of WS₂ particles, Ni-Co and Ni-Co/WS₂ coatings are characterized and summarized in Figure 4. WS₂ particles show diffraction peaks at 14°, 33°, 40°, 49° and 58°, which are consistent with the (002), (100), (103), (106) and (110) orientations of hexagonal WS₂. Both Ni-Co and Ni-Co/WS₂ samples exhibit distinct (0002) hcp/(111) fcc growth orientation with an intense peak at $2\theta \approx 44^\circ$. The Ni-Co/WS₂ sample also has an obvious peak at $2\theta = 14^\circ$, confirming the successful inclusion of WS₂ in the coating. Using the Scherrer equation and observed diffraction peak widths, the mean grain sizes of Ni-Co/WS₂ 7.1 wt.% deposits can be calculated as 14 ± 2 nm.

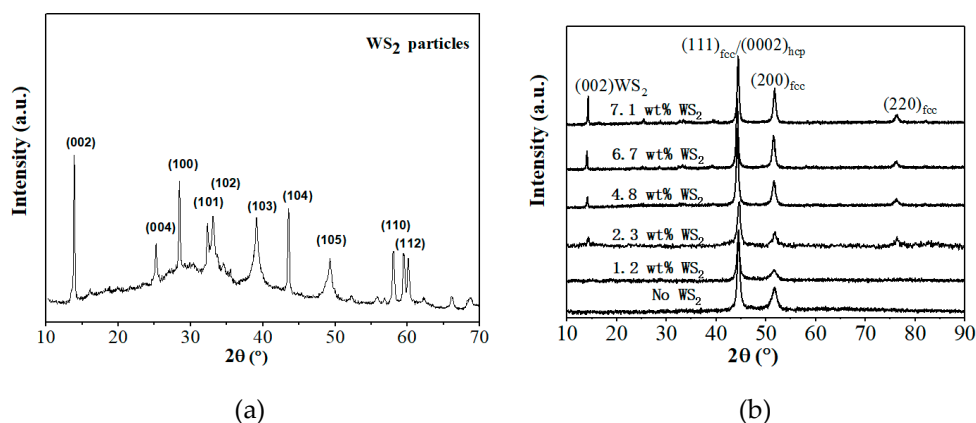


Figure 4. XRD patterns of (a) WS₂ particles and (b) Ni-Co/WS₂ samples with different WS₂ contents.

3.3. Compositional Analysis

The composition of electrodeposited coatings was examined by EDS. It can be seen in Figure 5 that the obtained coatings show a cobalt percentage in the range 35%–46%, which is much higher than the percentage of Co in the solutions. The trend is in consistency with the results in other Ni-Co electrodeposition systems [22]. The increment of the WS₂ particles in bath is found to lower the Co/Ni + Co ratio in coating, which is related to the electrochemical polarization caused by particle adsorption on the electrode [23].

Figure 5b shows that the weight percentage of WS₂ particles in coating increases with the increasing of the WS₂ concentration in bath, reaching a maximum WS₂ content of 7.1 wt.% at a particle concentration of 15 g L^{−1}. There is an optimal particle concentration in this experiment, as a further increase of WS₂ concentration leads to particle agglomeration and sedimentation in solution.

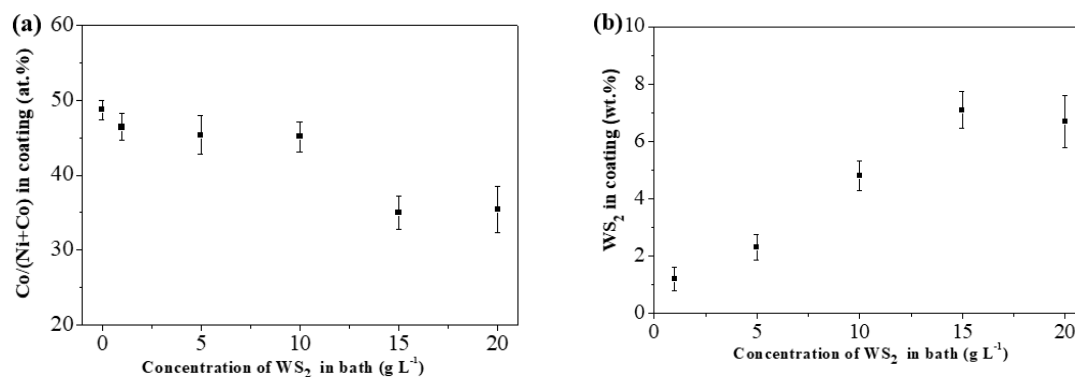


Figure 5. (a) The mol ratio of Co/(Co + Ni) and (b) the content of WS₂ particles in coating versus the concentration of WS₂ in solution.

3.4. Tribological Performance

Figure 6 shows the coefficient of friction (COF) versus time for samples having different WS₂ contents. The COF of the Ni–Co coating fluctuates within the range of 0.45 to 0.55 during the friction test. In contrast, the Ni–Co/WS₂ 1.2 wt.% sample exhibits a lower COF of 0.15 in the initial 300 s, but followed by a slow rise to the range of 0.45–0.55 that is close to the COF of pure Ni–Co coating. Notably, the Ni–Co/WS₂ 7.1 wt.% sample displays a stable low COF value of 0.16 for 1000 s, indicating the effective role of WS₂ lubricants on reduction of friction.

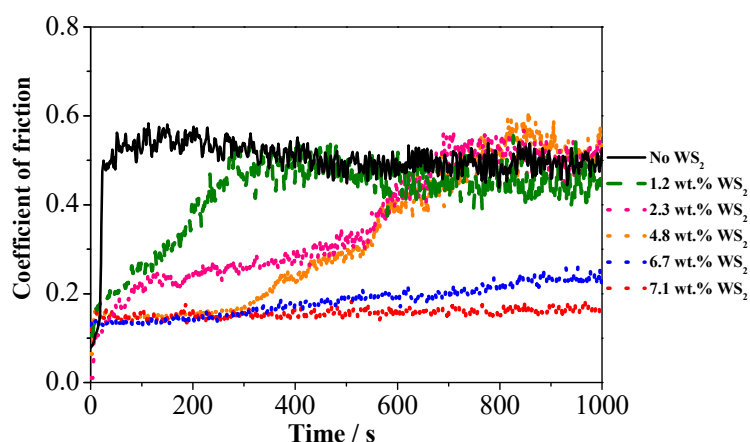


Figure 6. Relationship between friction coefficient and sliding time for the Ni–Co/WS₂ with different WS₂ contents.

The surface morphology and composition of wear tracks were examined by SEM and EDS respectively. Scoring wear can be found on the pure Ni–Co coating after wear test of 1000 s, as shown in Figure 7. The Ni–Co/WS₂ 1.2 wt.% composite coating presents a similar wear track surrounded by lots of debris particles. It is worth noting that the surface protrusions of the electrodeposited coating are fragile and easily fractured during the friction process. With the increasing of WS₂ content in coating the wear gradually became less severe and finally changed to galling in the case of Ni–Co/WS₂ coatings with WS₂ content 2.3 wt.% and higher. The wear degree of the Ni–Co/WS₂ coating decreases with the increase of WS₂ content in coating. The Ni–Co/WS₂ 7.1 wt.% sample shows only a narrow abrasive wear track with few debris particles. As listed in Table 1, the wear track of Ni–Co coating is composed of 22.1 wt.% Ni, 21.9 wt.% Co, 23.0 wt.% O and 33.0 wt.% Fe. The wear track of the Ni–Co/WS₂ 7.1 wt.% sample contains a higher WS₂ content than that of the resting area on the coating, suggesting that WS₂ has a high adhesion ability to the sliding surface. The wear track of the Ni–Co/WS₂ 7.1 wt.% sample shows a smaller oxygen content of 1.8 wt.% compared to that of pure

Ni-Co coating. On the one side, the release of WS₂ from the coating matrix reduces frictional heat on the mating surfaces, and on the other, the formation of compact WS₂ rich tribofilm separates the coating from the air. These two effects lead to a low degree of oxidation.

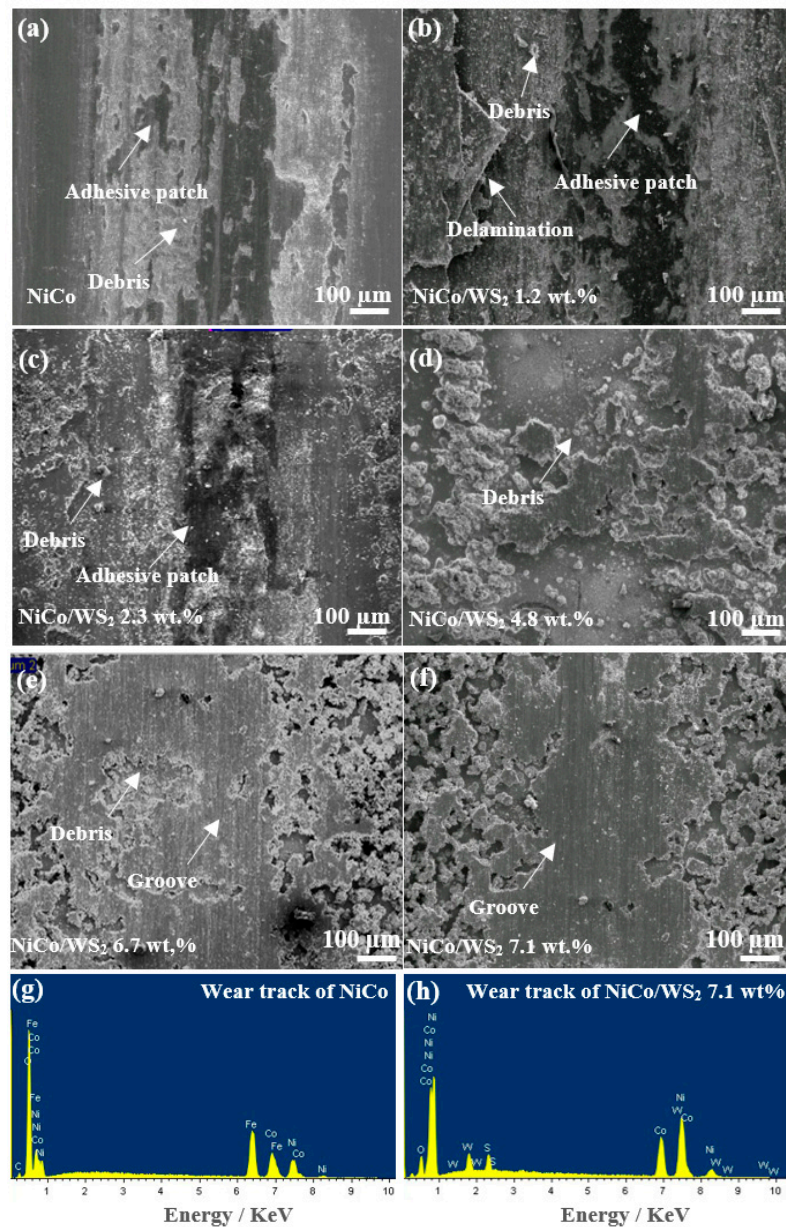


Figure 7. (a–f) SEM images of the wear tracks on various Ni–Co/WS₂ coatings; (g–h) EDS spectra of the wear tracks on Ni–Co coating and Ni–Co/WS₂ 7.1 wt.% coating.

Table 1. Composition of wear tracks on Ni–Co and Ni–Co/WS₂ coatings after friction testing.

Element (wt.%)	Ni-Co	Ni-Co/WS ₂ 1.2 wt.%	Ni-Co/WS ₂ 2.3 wt.%	Ni-Co/WS ₂ 4.8 wt.%	Ni-Co/WS ₂ 6.7 wt.%	Ni-Co/WS ₂ 7.1 wt.%
Ni K	22.1	28.5	47.3	48.5	57.5	58.2
Co K	21.9	25.7	40.9	41.6	31.6	31.3
W M	–	0.9	1.5	4.4	5.8	6.9
S K	–	0.3	0.5	1.5	2.1	1.9
O K	23.0	17.1	4.8	4.0	3.0	1.8
Fe K	33.0	27.5	5.1	–	–	–

Figure 8 shows a comparison between Ni-Co coating and Ni-Co/WS₂ coating in the wear volume in the friction test. Ni-Co coating has a wear volume of $9.5 \times 10^{-3} \text{ mm}^{-3}$. The wear volume of the Ni-Co/WS₂ 1.2 wt.% coating is as high as $2.0 \times 10^{-2} \text{ mm}^{-3}$ which is related to delamination failure. It is evident that the amount of codeposited WS₂ particles is important for improving the wear resistance of the Ni-Co coating when sliding against the steel ball, as indicated by lower volume of $6.0 \times 10^{-3} \text{ mm}^{-3}$ and $5.5 \times 10^{-3} \text{ mm}^{-3}$ for the Ni-Co/WS₂ 6.7 wt.% and Ni-Co/WS₂ 7.1 wt.% coatings.

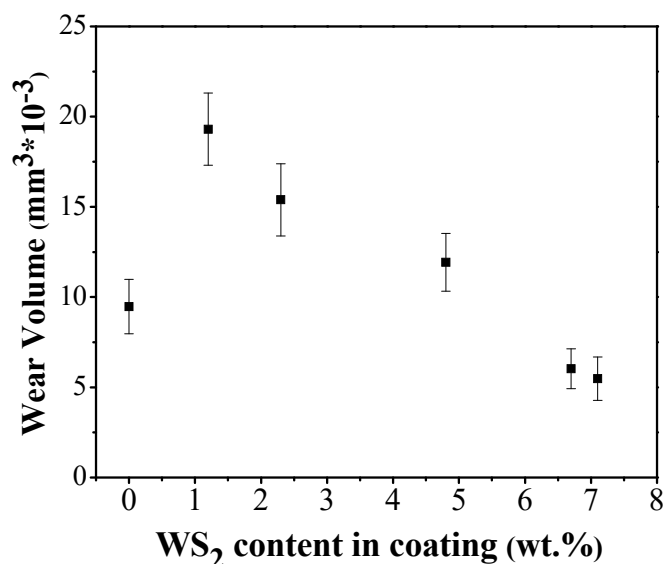


Figure 8. Comparison of wear volumes of Ni-Co coating and Ni-Co/WS₂ coatings with different WS₂ contents.

A proper run-in period is vital to the friction and wear performance of the electrodeposited coatings. Due to lack of sufficient solid lubricants, Ni-Co, Ni-Co/WS₂ 1.2 wt.% and Ni-Co/WS₂ 2.3 wt.% are not well run-in when sliding against the counter steel ball. For the Ni-Co/WS₂ coatings with WS₂ content 6.7 wt.% and higher, solid lubricants are reserved within the Ni-Co matrix and gradually released to the friction surfaces for lubrication, resulting in fast run-in and low friction and fundamentally inhibiting excessive operating temperatures and scuffing damage especially at high speeds.

Figure 9 the surface morphologies of counter steel balls after sliding tests. A clear wear scar is observable on the wear track of the steel ball after sliding against Ni-Co coating. Lots of wear debris is observed on the counter ball after sliding against the Ni-Co/WS₂ 1.2 wt.% coating, which derives from the breakdown of the nodular microstructures in the coating. In contrast, there is a smooth wear track on the counterpart ball after friction against the Ni-Co/WS₂ 7.1 wt.% coatings, suggesting effective lubrication by WS₂ from the coating.

For the Ni-Co coating, the adhesion force between the counterpart ball and the Ni-Co alloy surface is strong; debris particles generated during the friction test are crushed and piled up along the wear scar, i.e., not over-rolled. The wear particles slide firmly on the surface and turn into incomplete tribofilm during a long sliding time.

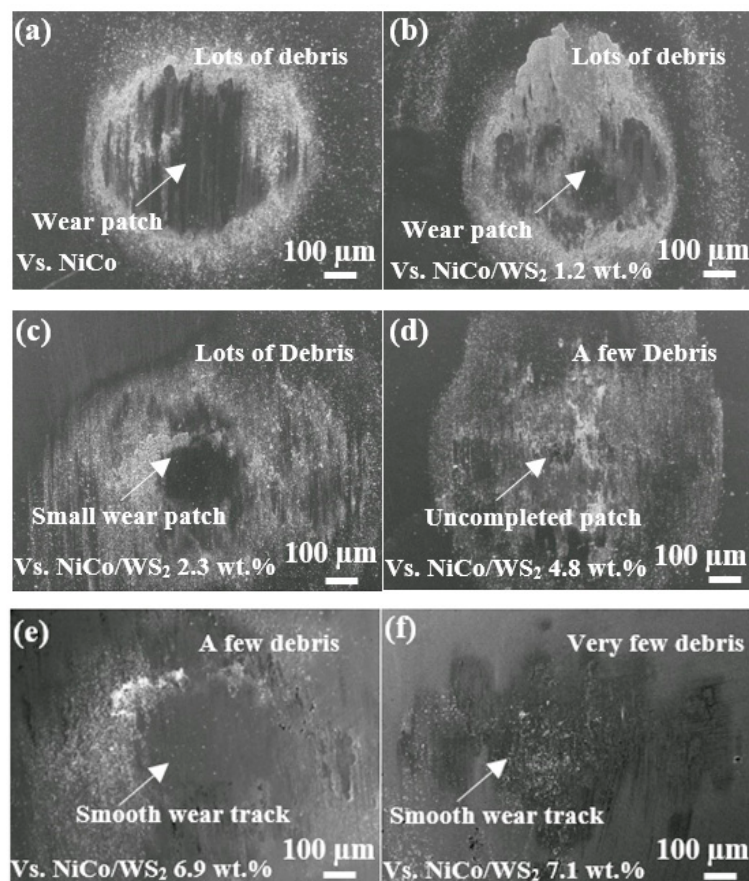


Figure 9. SEM images of counter balls after friction tests against (a) Ni–Co coating and Ni–Co/WS₂ coatings with different WS₂ contents: (b) 1.2 wt.%, (c) 2.3 wt.%, (d) 4.8 wt.%, (e) 6.7 wt.% and (f) 7.1 wt.%.

Due to the lamellar structure of WS₂, the inclusion of WS₂ particles into the Ni–Co coating significantly reduces the shear force (τ) causing a decrease in the friction coefficient, especially when a smooth lubricating layer is produced. The reconditioning and self-lubricating processes of Ni–Co/WS₂ coating is proposed as follows. Once friction starts, the movement of the counterpart ball will impose high shear stress on the contact area, resulting in severe deformation in the coating surface. Then the embedded WS₂ nanoparticles in the coating can release from their fixed positions to enter the sliding surfaces. Some WS₂ lamellae will be exfoliated into fine particles, which are easily accumulated in the wear crevices or attached to the metal surface to form a densely packed super-lubricating layer. The lubricating layer not only firmly attaches to the coating surface, but also transfers to the counterpart, thus contributing to the excellent tribological properties such as low friction coefficient, good wear resistance and high oxidation resistance under dry sliding conditions without oil or grease.

3.5. Wettability

The wetting properties of electrodeposited surfaces are determined by the water contact angle test. As seen in Figure 10, the pure Ni–Co coating has a low WCA of 85°. With the WS₂ content increasing, the WCA of the Ni–Co/WS₂ coating significantly increases. The Ni–Co/WS₂ 7.1 wt.% coating shows an excellent superhydrophobicity as indicated by a high WCA of 156.9 deg.

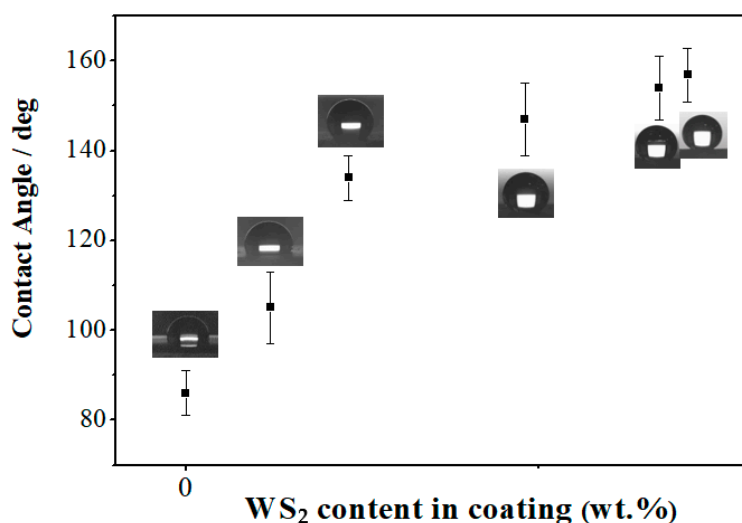


Figure 10. The variation in contact angle of water on the electrodeposited Ni-Co/WS₂ coatings against the concentrations of WS₂ in solution.

Figure 11 illustrates that the water droplet suspended on a needle tip is difficult to deposit on the coating even though it has been severely deformed. The water droplet rolls to one side when the needle tip approaches the sample surface, but can remain attached to the tip as the needle leaves the sample. This phenomenon indicates that the electrodeposited Ni-Co/WS₂ coating has a very low surface energy.

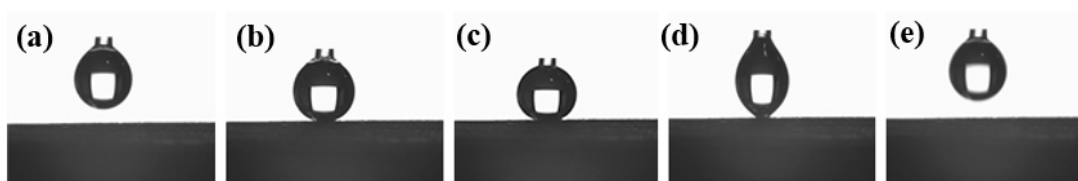


Figure 11. (a–e) Photographs illustrating water droplet does not adhere to the Ni-Co/WS₂ 7.1 wt.% surface: (a) a needle with suspended water droplet is set on the top of the Ni-Co/WS₂ coating; (b) the water droplet touches the surface of the coating with a low approaching velocity; (c) the water droplet become rounder as the needle further approach; (d) the water droplet is deformed heavily when the needle is separating from surface; (e) the water droplet is away from the coating after separation.

As well known, surface wettability is determined by chemical composition and surface structure, and can be described by either the Wenzel [24] or Cassie–Baxter model [25]. The Ni–Co surface has a WCA below 90° and is intrinsically hydrophilic. According to Wenzel’s model, the wettability of intrinsic hydrophilic surface should be enhanced as the roughness increases, which is obviously not applicable for the electrodeposited Ni-Co/WS₂ coatings. Cassie–Baxter’s model is commonly used to predict the hydrophobicity when air is trapped between the solid surface and the liquid droplet. The Ni-Co/WS₂ surfaces have a double-rough structure consisting of submicron asperities on micron-scale protrusions as illustrated in Figure 12; therefore, when these coatings are subjected to a liquid droplet, air bubbles are trapped and retained within asperities on the surface, maintaining the hydrophobic Cassie–Baxter state. The dual scale roughness has already been applied as the most commonly used criterion for superhydrophobic solid surface in the Cassie–Baxter state [26].

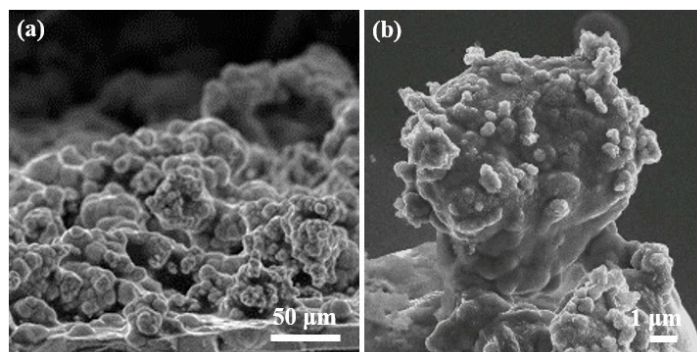


Figure 12. (a) Low- and (b) high- magnification SEM images of the cross-section of a Ni-Co/WS₂ 7.1 wt.% coating.

4. Conclusions

Ni-Co/WS₂ nanocomposite coatings have been successfully fabricated using a rapid one-pot electrodeposition route. The increase of the WS₂ content plays an important role in lowering the friction coefficient of the electrodeposited coating against steel to 0.16. The analysis of the morphology and composition of wear scars reveal that WS₂ strongly adheres to the sliding interfaces for effective lubrication rather than being squeezed out. Adequate levels of WS₂ in the coating could enable the formation of a compact, WS₂-rich tribofilm on the sliding interfaces that accounts for the ultra-low friction coefficient and high oxidation resistance. Moreover, the hierarchical rough Ni-Co/WS₂ composite coating exhibits excellent superhydrophobicity with a high WCA of 158°.

Author Contributions: Conceptualization, Y.H. and S.W.; Methodology, Y.H.; Investigation, Y.H. and W.S.; Formal Analysis, Y.H. and S.W.; Writing—Original Draft Preparation, Y.H.; Writing—Review and Editing, Y.H., S.W., W.S., P.A.S.R. and F.C.W.; Supervision, S.W., P.A.S.R. and F.C.W.; Project Administration, Y.H.; Funding Acquisition, Y.H.

Funding: This research was funded by National Natural Science Foundation of China (No. 11802077).

Conflicts of Interest: The authors declare no conflict of interest.

References

1. Tian, L.; Xu, J.; Xiao, S. The influence of pH and bath composition on the properties of Ni-Co coatings synthesized by electrodeposition. *Vacuum* **2011**, *86*, 27–33. [\[CrossRef\]](#)
2. Wang, L.; Gao, Y.; Xue, Q.; Liu, H.; Xu, T. Microstructure and tribological properties of electrodeposited Ni-Co alloy deposits. *Appl. Surf. Sci.* **2005**, *242*, 326–332. [\[CrossRef\]](#)
3. Go, E.; Ramirez, J.; Valle, E. Electrodeposition of Co-Ni alloys. *J. Appl. Electrochem.* **1998**, *28*, 71–79.
4. He, Y.; Wang, S.C.; Walsh, F.C.; Li, W.S.; He, L.; Reed, P.A.S. The monitoring of coating health by in situ luminescent layers. *RSC Adv.* **2015**, *5*, 42965–42970. [\[CrossRef\]](#)
5. Correia, A.N.; Machado, S.A.S. Electrodeposition and characterisation of thin layers of Ni-Co alloys obtained from dilute chloride baths. *Electrochim. Acta* **2000**, *45*, 1733–1740. [\[CrossRef\]](#)
6. Qiao, G.; Jing, T.; Wang, N.; Gao, Y.; Zhao, X.; Zhou, J.; Wang, W. High-speed jet electrodeposition and microstructure of nanocrystalline Ni-Co alloys. *Electrochim. Acta* **2005**, *51*, 85–92. [\[CrossRef\]](#)
7. Hibbard, G.D.; Aust, K.T.; Erb, U. Thermal stability of electrodeposited nanocrystalline Ni-Co alloys. *Mater. Sci. Eng. A* **2006**, *433*, 195–202. [\[CrossRef\]](#)
8. Ma, C.; Wang, S.C.; Walsh, F.C. Electrodeposition of nanocrystalline nickel-cobalt binary alloy coatings: A review. *Trans. IMF* **2015**, *93*, 104–112. [\[CrossRef\]](#)
9. Chen, W.X.; Tu, J.P.; Wang, L.Y.; Gan, H.Y.; Xu, Z.D.; Zhang, X.B. Tribological application of carbon nanotubes in a metal-based composite coating and composites. *Carbon* **2003**, *41*, 215–222. [\[CrossRef\]](#)
10. Akbarpour, M.R.; Alipour, S.; Safarzadeh, A.; Kim, H.S. Wear and friction behavior of self-lubricating hybrid Cu-(SiC + xCNT) composites. *Compos. Part B Eng.* **2019**, *158*, 92–101. [\[CrossRef\]](#)
11. Zhao, H.; Liu, L.; Hu, W.; Shen, B. Friction and wear behavior of Ni-graphite composites prepared by electroforming. *Mater. Des.* **2007**, *28*, 1374–1378. [\[CrossRef\]](#)

12. Sun, W.C.; Zhang, P.; Zhao, K.; Tian, M.M.; Wang, Y. Effect of graphite concentration on the friction and wear of Ni–Al₂O₃/graphite composite coatings by a combination of electrophoresis and electrodeposition. *Wear* **2015**, *342*, 172–180. [[CrossRef](#)]
13. He, Y.; Wang, S.C.; Walsh, F.C.; Chiu, Y.L.; Reed, P.A.S. Self-lubricating Ni-P-MoS₂ composite coatings. *Surf. Coat. Technol.* **2016**, *307*, 926–934. [[CrossRef](#)]
14. Redlich, M.; Gorodnev, A.; Feldman, Y.; Kaplanashiri, I.; Tenne, R.; Fleischer, N.; Genut, M.; Feuerstein, N. Friction reduction and wear resistance of electro-co-deposited inorganic fullerene-like WS₂ coating for improved stainless steel orthodontic wires. *J. Mater. Res.* **2008**, *23*, 2909–2915. [[CrossRef](#)]
15. Mai, Y.J.; Zhou, M.P.; Ling, H.J.; Chen, F.X.; Lian, W.Q.; Jie, X.H. Surfactant-free electrodeposition of reduced graphene oxide/copper composite coatings with enhanced wear resistance. *Appl. Surf. Sci.* **2018**, *433*, 232–239. [[CrossRef](#)]
16. García-Lecina, E.; García-Urrutia, I.; Díez, J.A.; Fornell, J.; Pellicer, E.; Sort, J. Codeposition of inorganic fullerene-like WS₂ nanoparticles in an electrodeposited nickel matrix under the influence of ultrasonic agitation. *Electrochim. Acta* **2013**, *114*, 859–867. [[CrossRef](#)]
17. Tudela, I.; Zhang, Y.; Pal, M.; Kerr, I.; Cobley, A.J. Ultrasound-assisted electrodeposition of thin nickel-based composite coatings with lubricant particles. *Surf. Coat. Technol.* **2015**, *276*, 89–105. [[CrossRef](#)]
18. Roy, D.; Das, A.K.; Saini, R.; Singh, P.K.; Kumar, P.; Hussain, M.; Mandal, A.; Dixit, A.R. Pulse current co-deposition of Ni–WS₂ nano-composite film for solid lubrication. *Mater. Manuf. Proc.* **2017**, *32*, 365–372. [[CrossRef](#)]
19. He, Y.; Sun, W.T.; Wang, S.C.; Reed, P.A.S.; Walsh, F.C. An electrodeposited Ni–P/WS₂ coating with combined super-hydrophobicity and self-lubricating properties. *Electrochim. Acta* **2017**, *245*, 872–882. [[CrossRef](#)]
20. Zhao, G.; Xue, Y.; Huang, Y.; Ye, Y.; Walsh, F.C.; Chen, J.; Wang, S. One-step electrodeposition of a self-cleaning and corrosion resistant Ni/WS₂ superhydrophobic surface. *RSC Adv.* **2016**, *6*, 439–443. [[CrossRef](#)]
21. Shi, L.; Sun, C.F.; Gao, P.; Zhou, F.; Liu, W.M. Electrodeposition and characterization of Ni–Co–carbon nanotubes composite coatings. *Surf. Coat. Technol.* **2006**, *200*, 4870–4875. [[CrossRef](#)]
22. Golodnitsky, D.; Yu, R.; Ulus, A. The role of anion additives in the electrodeposition of nickel–cobalt alloys from sulfamate electrolyte. *Electrochim. Acta* **2003**, *47*, 2707–2714. [[CrossRef](#)]
23. Gómez, E.; Pané, S.; Vallés, E. Electrodeposition of Co–Ni and Co–Ni–Cu systems in sulphate–citrate medium. *Electrochim. Acta* **2006**, *51*, 146–153. [[CrossRef](#)]
24. Wenzel, R.N. Resistance of solid surfaces to wetting by water. *Ind. Eng. Chem.* **1936**, *28*, 988–994. [[CrossRef](#)]
25. Cassie, A.B.D.; Baxter, S. Wettability of porous surfaces. *Trans. Faraday Soc.* **1944**, *40*, 546–551. [[CrossRef](#)]
26. Shirtcliffe, N.J.; McHale, G.; Newton, M.I.; Chabrol, G.; Perry, C.C. Dualscale roughness produces unusually water repellent surfaces. *Adv. Mater.* **2004**, *16*, 1929–1932. [[CrossRef](#)]

